Kramer, M. et al. "Towards reliable turbulence estimations with phase-detection probes: An adaptive window cross-correlation technique" Experiments in Fluids (2019) 60:2.
https://doi.org/10.1007/s00348-018-2650-9

Towards reliable turbulence estimations with phase-detection probes: An adaptive window cross-correlation technique

Matthias Kramer · Daniel Valero · Hubert Chanson · Daniel B. Bung

Received: 11.09.2018 / Accepted: 15.11.2018 / Published online: 26.11.2018

Abstract Air-water flow turbulence was derived from pseudo-instantaneous velocities measured with a dual-tip phase-detection probe. A new technique is proposed based upon adaptive time windows for cross-correlation analysis jointly with robust filtering criteria, allowing computation of velocity time series in highly-aerated flows. Each velocity estimation corresponded to a small group of bubbles or droplets. Stochastic synthetic velocity fields were generated to assess the limitations and uncertainties related to the proposed analysis. Subsequently, capabilities of the technique were demonstrated through an application to a real two-phase flow on a large-size stepped spillway.

Matthias Kramer*
The University of Queensland
School of Civil Engineering
Brisbane QLD 4072, Australia
E-mail: m.kramer@uq.edu.au
ORCID: 0000-0001-5673-2751

Daniel Valero
FH Aachen University of Applied Sciences
Hydraulic Engineering Section (HES)
Aachen 52066, Germany
E-mail: valero@fh-aachen.de
University of Liège (ULiège)
Hydraulics in Environmental and Civil Engineering (HECE)
ORCID: 0000-0002-7127-7547

Hubert Chanson
The University of Queensland
School of Civil Engineering
Brisbane QLD 4072, Australia
E-mail: h.chanson@uq.edu.au
ORCID: 0000-0002-2016-9650

Daniel B. Bung
FH Aachen University of Applied Sciences
Hydraulic Engineering Section (HES)
Aachen 52066, Germany
E-mail: bung@fh-aachen.de
ORCID: 0000-0001-8057-1193

Keywords Phase-detection dual-tip probe · Multiphase gas-liquid flow · Highly-aerated flow · Signal processing · Turbulence

1 Introduction

With classic instrumentation, significant limitations arise in gas-liquid and liquid-liquid flows with dispersed phase volume fractions over a few percent. Metrology accuracy impairment has forced researchers and engineers to use unique techniques for the study of multiphase flows. Phase-detection probes have been the preferred choice since the early work of Neal and Bankoff (1963). This instrumentation works upon the principle of changing conductivity or light refraction. When two tips are aligned along a streamline, the interfacial velocity may be derived (Herringe and Davis 1976).

Conductivity and optical fiber needle probes have allowed estimation of a wide range of interfacial flow properties through advanced post-processing, comprising flows with low void fractions (Kataoka et al 1986; Revankar and Ishii 1993) and highly-aerated flows (Cartellier and Achard 1991; Chanson and Toombes 2002; Felder and Chanson 2015). Cartellier (1998) achieved an instantaneous velocity estimation by taking the phase function gradients of a single-tip signal into account, whereas indirect turbulence estimations were based on the shape of the cross-correlation function using a dual-tip probe (Chanson and Toombes 2002). Chang et al (2003) used an individual event detection technique to measure void fraction and velocity with a single-tip optical fiber probe. While the techniques of Cartellier (1998) and Chang et al (2003) hold large uncertainties for high-velocity engineering applications, the indirect estimation of the turbulence intensity includes different sources of errors. To date, direct estimation of velocity fluctuations remained undetermined, although every phase change detected by two tips could, ultimately, yield some instantaneous interfacial velocity estimation.

In this study, the capability of a cross-correlation technique with an adaptive time window is explored. The signal of a phase-detection dual-tip probe was segmented into very short windows, each containing groups of a few bubbles/droplets. Cross-correlation analyses, combined with the implementation of filtering criteria, yielded reliable pseudo-instantaneous interfacial velocities. The proposed technique is applicable to various gas-liquid flows (bubbly flows, sprays and intermediate flow regimes) and has been analysed on a fundamental basis through stochastic signals. Subsequently, practical capabilities are demonstrated by means of a large-size stepped spillway case study, presenting direct estimations of velocity fluctuations and turbulence spectra from dual-tip conductivity probe signals.

2 Adaptive window cross-correlation technique

2.1 Signal segmentation and velocity estimation

The two tips of a phase-detection needle probe, denoted as leading and trailing tips, allow simultaneous phase detection at two fixed locations, separated by a streamwise distance Δx (Figure 1). The probe yields two signals at a sampling

rate f_s, that – ideally – would be identical, but shifted by Δt. A simple method to obtain "water" and "air" phase signals from the raw voltage output is the single-threshold technique (Cartellier and Achard 1991), which results in binary time series (S_1 and S_2, see Figure 1), taking the value 0 (water) and 1 (air).

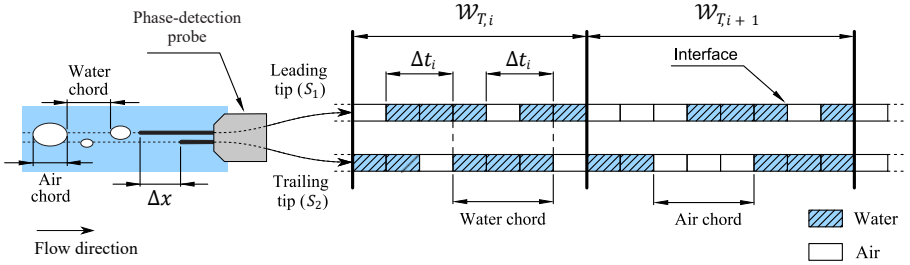

Fig. 1 Intrusive dual-tip phase-detection probe and simplified signals (Toombes 2002) after application of a single-threshold filter; correlation windows with $N_p = 2$ particles

The probe signals can be divided based on a defined number of bubble-droplet events N_p. Herein, a segment started when air was detected by the leading tip and finished after a number N_p of water chords. Each segment could yield a different time window $\mathcal{W}_{T,i}$ (Figure 1). The time shift Δt_i for an arbitrary $\mathcal{W}_{T,i}$ was obtained through the cross-correlation between $S_{1,i}$ and $S_{2,i}$:

$$R_{12,i}(\tau) = \frac{\sum_{t=t_i}^{t_i+\mathcal{W}_{T,i}} (S_1(t) - \overline{S_{1,i}}) \times (S_2(t+\tau) - \overline{S_{2,i}})}{\sqrt{\sum_{t=t_i}^{t_i+\mathcal{W}_{T,i}} (S_1(t) - \overline{S_{1,i}})^2} \times \sqrt{\sum_{t=t_i}^{t_i+\mathcal{W}_{T,i}} (S_2(t+\tau) - \overline{S_{2,i}})^2}} \quad (1)$$

with τ the time lag, t_i the starting time step of the segment i and, by definition, $R_{12,i} \leq 1$. The peak of $R_{12,i}$ indicated the time delay $T_i = \arg max(R_{12,i})$ for which both signals were best correlated, allowing to approximate $\Delta t_i \approx T_i$. Hence, a time-averaged longitudinal velocity, representative of the window time $\mathcal{W}_{T,i}$, was computed as:

$$[\overline{u}]_{t_i}^{t_i+\mathcal{W}_{T,i}} \approx u_i = \frac{\Delta x}{T_i} \quad (2)$$

Physically, the minimum window size is $\mathcal{W}_{T,i} \sim \Delta t_i$, which is the necessary window to hold a phase change, and would result in instantaneous velocity at a time $t = t_i + \mathcal{W}_{T,i}/2$. Because of differences between bubbles/droplets detected by leading and trailing tips, a larger N_p (and thus, $\mathcal{W}_{T,i}$) is necessary for a robust velocity estimation. In the present study, S_1 and S_2 were broken into non-overlapping segments, encompassing a small number of particles N_p, which were determined for both studied cases through a sensitivity analysis.

2.2 Filtering criteria

For each time window i, a pseudo-instantaneous velocity u_i could be estimated. The accuracy of an instantaneous measurement was dependent on the interfacial

information contained in both signals, which became critical when using short correlation windows. To ensure the reliability of a velocity estimation, two filtering criteria and an outlier detection method were applied.

The first criterion implied a minimum similarity between both segments ($S_{1,i}$ and $S_{2,i}$), as quantified by the cross-correlation technique:

$$R_{12,i,\max} > 0.5 \tag{3}$$

where $R_{12,i,\max}$ is the maximum cross-correlation coefficient. Because of the existence of multiple peaks in the cross-correlation function, a SPR (secondary peak ratio) coefficient was introduced, defined as the ratio of the second tallest peak to the first tallest peak of the cross-correlation function:

$$\mathrm{SPR}_i = \frac{R_{12,i,2^{\mathrm{nd}}\max}}{R_{12,i,\max}} < 0.6 \tag{4}$$

To compute $R_{12,i,2^{\mathrm{nd}}\max}$, the neighboring points of each time lag were analysed and only isolated peaks were considered. The SPR is the reciprocal of the detectability used in Particle Image Velocimetry (PIV) and values of $\mathrm{SPR}_i < 0.6$ are consistent with well established thresholds (Keane and Adrian 1990).

The time series of pseudo-instantaneous velocities may also include outliers. The despiking method of Goring and Nikora (2002), as modified by Wahl (2003), was applied to reduce the number of outliers without taking velocity derivatives into account, thus establishing an upper and lower threshold for admissible velocities.

3 Case studies

3.1 Stochastic velocity fields

Stochastic velocity fields can be generated by means of the Langevin equation, similar to Bung and Valero (2017). The Langevin equation was first proposed as a stochastic model for the velocity of a particle subject to Brownian movement (Langevin 1908). The equation, governing a stochastic process u^* with mean zero and integral time-scale T_x, can be written as (Pope 2000):

$$u^*\left(t+\delta t\right) = u^*(t)\left(1-\frac{\delta t}{T_x}\right) + u^*_{rms}\left(\frac{2\,\delta t}{T_x}\right)^{1/2}\xi(t) \tag{5}$$

for time steps $\delta t \ll T_x$, where $\xi(t)$ is a standardized Gaussian random variable. The modelled velocity u^* represents the fluctuating particle velocity u' ($u^* \sim u'$) and can be superimposed to a time-averaged velocity U, which can also serve to estimate the turbulence intensity $Tu_x = u'_{rms}/U = \sqrt{\overline{(u')^2}}/U$. The velocities computed using Equation (5) satisfy a $-5/3$ spectra energy decay. The strength of this approach relies on the possibility to generate physically based, controlled turbulent velocity fields.

Random patterns of synthetic droplets with 70% and 90% air volume fractions (C) were transported with generated time-dependent velocities (see Table 1) in the streamwise direction. No motion in normal or transverse direction was taken

into account, thus corresponding to a flow with homogeneous, anisotropic turbulence. The particles were ellipsoidal with a shape factor of 0.7, implying a longer streamwise dimension than vertical and transverse dimensions. The streamwise mean dimension was set to $d_{\mathrm{mean}} = 3$ mm and followed a Gamma distribution with parameters $\alpha = 1.5$ and $\beta = 1$. The parameters α and β were selected to be representative for distributions observed in flows down stepped spillways (Chanson and Toombes 2002; Toombes 2002). Particles were transported with the same velocity as the surrounding fluid (no-slip) and no interactions (i.e. breakup and coalescence) were simulated. Overlapping particles had no effect on evaluated quantities.

A virtual phase-detection probe with two tips was positioned in the centre of the particle pattern, measuring whether a tip detected air or water, resulting in a phase fraction signal for each tip. The tips of the virtual probe were ideally thin and had a longitudinal separation of $\Delta x = 4$ mm, while the vertical and transversal separations were set to zero. The probe was sampled for a duration $t_s = 10$ s at a sampling frequency $f_s = 20$ kHz.

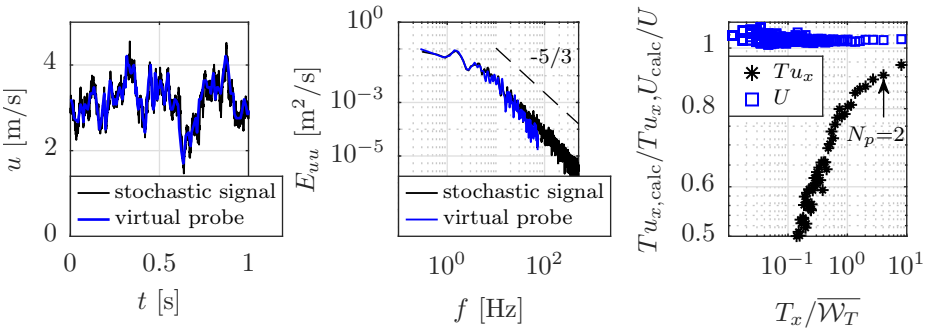

Fig. 2 Comparison between the generated flow field (stochastic signal) and the estimation of the proposed adaptive window cross-correlation technique (virtual probe); results correspond to $N_p = 2$ particles (except Figure 2 C), $U = 3$ m/s, $Tu_x = 0.2$ and $C = 0.7$ (Table 1).
(A, left) Time series of stochastic and measured velocities; only 1 second is shown for clarity.
(B, middle) One-dimensional velocity spectra (E_{uu}).
(C, right) Accuracy of the estimations versus ratio of the integral time scale T_x and the mean time window $\overline{\mathcal{W}_T}$ (variable N_p).

The virtual probe signals were processed with the adaptive window cross-correlation technique. Figure 2A shows the stochastic signal time series and velocities detected with the virtual probe for $N_p = 2$ particles, $U = 3$ m/s and $Tu_x = 0.2$. Because of the random distribution of particles, velocity data were unevenly distributed in the time domain and some data gaps were observed. A linear interpolation technique was used to fill missing data and to resample the signal at equidistant time intervals. One-dimensional velocity spectra E_{uu}, as defined by Pope (2000), showed a good agreement for all cases (Figure 2B), both at large and small scales, hence endorsing the proposed methodology. Note that the cut-off frequency of the virtual probe was determined by the number of interfaces hitting the probe tips or the bubble/droplet frequency F, respectively.

Figure 2C shows the ratio of the integral time scale to the mean time window ($T_x/\overline{\mathcal{W}_T}$, variable N_p) as function of the accuracy of estimated quantities, defined as U_{calc}/U and $Tu_{\mathrm{x,calc}}/Tu_x$. The estimation of the time-averaged velocity was relatively identical, regardless of the number of segments, whereas turbulence estimations showed a power-law scaling in terms of $T_x/\overline{\mathcal{W}_T}$ for $0.01 < T_x/\overline{\mathcal{W}_T} < 1$, with an asymptotic behaviour above unity. Additionally, signals with sampling times $t_s = 30$ s and 60 s indicated that the accuracy for the idealised flow conditions did not increase with longer sampling times, but this may not hold true for real applications (Toombes 2002; Felder and Chanson 2015).

Relative errors were small but increased with decreasing F and increasing Tu_x (Table 1). Partly, there is a limit to the accuracy that can be obtained, despite the simplicity of the case. Given that the particles are randomly distributed in the flow and that they approach the probe at high and low velocities, a greater number of particles impacts the tips during periods of high velocities, resulting in some velocity overestimation. For the cases considered (Table 1), this represented a maximum overestimation of the time-averaged velocity below 10%. This error is inherently linked to intense velocity fluctuations and, naturally, has a larger effect on the estimation of turbulence intensities compared to the estimation of time-averaged velocities.

Table 1 Results for the virtual probe sampling of the stochastic velocity fields; $N_p = 2$; dist = distribution.

Flow description			Particle characteristics				Sampling properties			Errors	
U	Tu_x	T_x	C	F	dist	d_{mean}	t_s	f_s	Δx	U	Tu_x
[m/s]	[-]	[s]	[-]	[1/s]	[-]	[mm]	[s]	[kHz]	[mm]	[%]	[%]
3.0	0.1	0.06	0.7	142	Gamma	3	10	20	4	0.9	1.9
3.0	0.1	0.06	0.9	56	Gamma	3	10	20	4	1.4	2.3
3.0	0.2	0.06	0.7	140	Gamma	3	10	20	4	3.0	9.5
3.0	0.2	0.06	0.9	57	Gamma	3	10	20	4	3.8	10.0
3.0	0.3	0.06	0.7	144	Gamma	3	10	20	4	7.6	11.7
3.0	0.3	0.06	0.9	58	Gamma	3	10	20	4	9.8	18.7

U, streamwise time-averaged velocity; Tu_x, turbulence intensity; T_x, integral time scale; C, void fraction; F, bubble/droplet count rate; dist, distribution; d_{mean}, streamwise dimension; t_s, sampling duration; f_s, sampling frequency; Δx, streamwise tip separation

3.2 Large-size stepped spillway

The case study demonstrated the capabilities of the technique in a real large-size application, where the signals differed from ideal signals. The highly turbulent free-surface flow down a stepped spillway can be classified into three different flow regimes, including nappe flow at low flow rates, transition flow at intermediate discharges and skimming flow for design discharges (Chanson 2001). Flows on stepped chutes are non-aerated at the spillway crest and aerated in the downstream part (Figure 3), exhibiting a broad range of void fractions C, which include the bubbly flow region next to the pseudo-bottom ($C < 0.3$), the intermediate region

($0.3 < C < 0.7$) and the spray region in the upper part of the flow ($C > 0.7$) (Chanson and Toombes 2002; Toombes 2002; Zhang 2017).

Experiments were undertaken in the fully aerated flow of a stepped chute with a slope of $\theta = 45°$, consisting of 12 steps with a length $l = 0.1$ m and a height $h = 0.1$ m (symmetric triangular cavity shape). Further description of the facility can be found in Zhang (2017). A dual-tip conductivity phase-detection probe (inner diameter: 0.25 mm, outer diameter: 0.8 mm, Δx: 4.7 mm) was mounted at the channel's centreline, at the 8^{th} step edge (Figure 3A). The sampling rate and duration were 20 kHz and 90 s respectively. The dimensionless discharge was $d_c/h = 1.1$, where d_c is the critical depth $d_c = (q^2/g)^{1/3}$, g is the gravitational acceleration and q the specific water discharge $q = 0.11$ m^2/s, corresponding to skimming flow conditions and a Reynolds number of $Re = 4\ q/\nu = 4.4\ \times 10^5$, where ν is the kinematic viscosity of water.

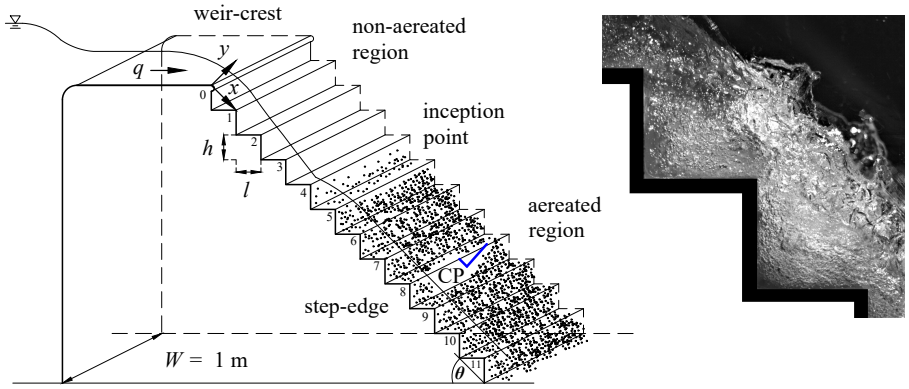

Fig. 3 Schematic of the experimental setup and high-speed image
(A, left) Broad crested weir and stepped spillway; q: specific discharge; l: step length; h: step height; θ: spillway slope; W: channel width; x: longitudinal direction; y: vertical direction; CP: phase-detection conductivity probe.
(B, right) Snapshot of the aerated flow, recorded with a Phantom v2011 high-speed camera; step-edges 4-6; $d_c/h = 1.1$; flow direction from top left to bottom right.

The computations of U and Tu_x were performed using the adaptive window cross-correlation technique. Because of real two-phase flow signals, which included probe-interface interaction and a non-zero probability that bubbles/droplets are detected by one tip only, a value of $N_p = 5$ was used. This choice was based on a balance between the percentage of accepted data and the error on the turbulence estimations.

The distribution of interfacial velocities at the step edge followed a smooth power-law profile (Figure 4A). The vertical profile of the turbulence intensity Tu_x (Figure 4A) had the shape of classic velocity fluctuations over rough channel beds, similar to PIV measurements of Amador et al (2006) ($q = 0.11$ m^2/s, step 5.1, $\theta = 51.3°$, $h = 0.05$ m, non-aerated region). Intensities were relatively large, most likely related to turbulence modulation produced by the dispersed phase dynamics

(Chanson and Toombes 2002). Tu_x was almost constant for $C \geq 0.5$, which could correspond to 'frozen' fluctuations of ejected particles in the spray region, as hinted by Zhang (2017).

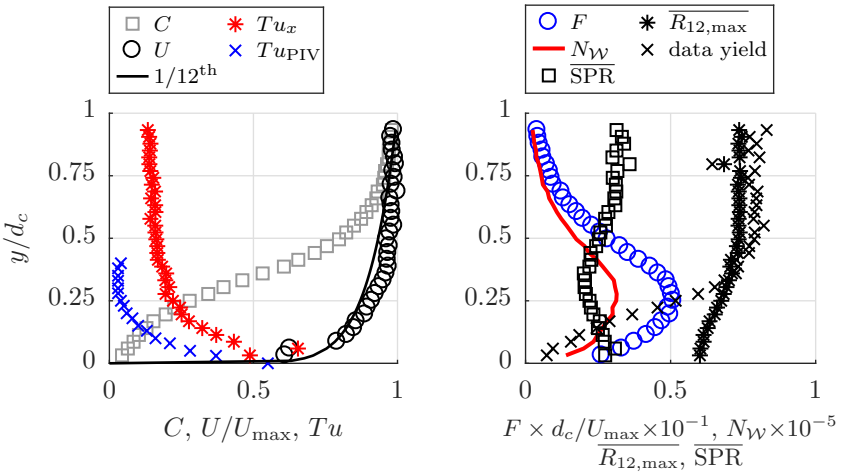

Fig. 4 Adaptive window cross-correlation technique applied to a stepped spillway flow. (A, left) Void fraction (C), interfacial velocity (U) dimensionless by the maximum cross-sectional velocity ($U_{\max}$), $1/12^{\text{th}}$ power law, air-water turbulence intensity (Tu_x), turbulence intensity from PIV measurements (Tu_{PIV} from non-aerated region of Amador et al 2006). (B, right) Dimensionless bubble count rate (F), number of windows ($N_{\mathcal{W}}$), maximum correlation coefficient ($\overline{R_{12,\max}}$), secondary peak ratio ($\overline{\text{SPR}}$) and fraction of non-rejected data (after filtering, data yield).

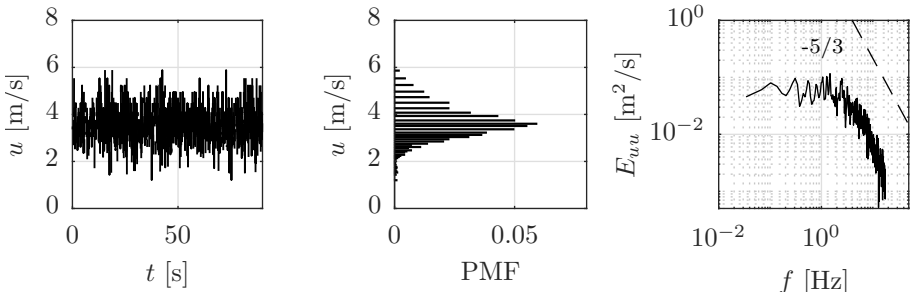

Fig. 5 Pseudo-instantaneous air-water flow variables at an elevation of $y/d_c = 0.25$; $C = 0.35$; $F = 175$ Hz.
(A, left) Time series of interfacial velocities.
(B, middle) Probability mass function (PMF).
(C, right) One-dimensional velocity spectrum (E_{uu}).

The measurement accuracy was linked to $\overline{\text{SPR}}$, $\overline{R_{12,\max}}$ (calculated as mean values) and the data yield, defined as the fraction of non-rejected data (Figure 4B). The lowest accuracy was found next to the step edge, whereas it was highest within the intermediate/upper region above the shear layer. This was related to (1) the number of windows per signal ($N_{\mathcal{W}}$, Figure 4B), being proportional to the bubble/droplet count rate F, and (2) the existence of intense transverse and normal fluctuations close to the step edges, inducing oblique impacts with the probe tips.

The probability mass function (PMF) of a representative velocity time series ($y/d_c = 0.25$, Figures 5A and 5B) followed a Gaussian distribution but had a sparse resolution for velocities greater than 4 m/s, suggesting that a higher sampling rate should be used for future measurements. The one-dimensional velocity spectrum (E_{uu}) showed an energy transfer like a Kolmogorov-type spectrum in the inertial subrange (Figure 5C). Note that there is an ongoing discussion related to the slope of the spectrum in gas-liquid flows and researchers have reported slopes of -3, -8/3 and -5/3 (Joshi et al 2017). Previous studies were conducted within the bubbly flow regime, which is characterised by low void fractions, typically not exceeding a few percent. The new technique allows to compute the spectrum in highly-aerated flows ($0.1 < C < 0.9$), providing the basis for the study of turbulence in high-velocity air-water flows.

4 Conclusion

This study presented a novel adaptive window cross-correlation technique for processing dual-tip phase-detection probe signals in multiphase gas-liquid flows. Cross-correlation analyses were performed on relatively short time windows, yielding pseudo-instantaneous interfacial velocities. The pseudo-instantaneous velocities were an estimate, averaged over the number of encompassed bubbles/droplets N_p.

A probabilistic analysis based on stochastic velocity fields confirmed the capabilities of the technique and shed light into measurement uncertainty. The proposed method was used to characterise the air-water flow down a stepped spillway. For the first time, velocity time series and turbulence spectra in highly-aerated flows were deduced from phase-detection probe measurements, hinting some energy transfer similar to a Kolmogorov-type spectrum. Altogether, the new method allowed the use of a dual-tip phase-detection probe to estimate time series of pseudo-instantaneous air-water velocities and associated flow variables.

Acknowledgements The authors thank Jason Van Der Gevel and Stewart Matthews (The University of Queensland) for the technical assistance and Dr Antonio Amador for sharing his turbulence dataset. The fruitful discussions with Uriah Gravois are acknowledged. Matthias Kramer was supported by DFG grant No. KR 4872/2-1.

References

Amador A, Sánchez-Juny M, Dolz J (2006) Characterization of the Nonaerated Flow Region in a Stepped Spillway by PIV. Journal of Fluids Engineering 128:1266–1273

Bung DB, Valero D (2017) FlowCV - An open source toolbox for computer vision applications in turbulent flows. In: Proceedings of the 37th IAHR World Congress, Kuala Lumpur, Malaysia
Cartellier A (1998) Measurement of gas phase characteristics using new monofiber optical probes and real-time signal processing. Nuclear Engineering and Design 184(2-3):393–408
Cartellier A, Achard J (1991) Local phase detection probes in fluid/fluid two-phase flows. Review of Scientific Instruments 62(2):279–303
Chang KA, Lim HJ, Chin BS (2003) Fiber optic reflectometer for velocity and fraction ratio measurements in multiphase flows. Review of Scientific Instruments 74:3559–3564
Chanson H (2001) The Hydraulics of Stepped Chutes and Spillways. Balkema Publishers
Chanson H, Toombes L (2002) Air–water flows down stepped chutes: turbulence and flow structure observations. International Journal of Multiphase Flow 28(11):1737–1761
Felder S, Chanson H (2015) Phase-detection probe measurements in high-velocity free-surface flows including a discussion of key sampling parameters. Experimental and Thermal Fluid Science 61:66–79
Goring DG, Nikora VI (2002) Despiking Acoustic Doppler Velocimeter Data. Journal of Hydraulic Engineering 128:117–126
Herringe RA, Davis MR (1976) Structural development of gas-liquid mixture flows. Journal of Fluid Mechanics 73:97–123
Joshi JB, Nandakumar K, Evans GM, Pareek VK, Gumulya MM, Sathe MJ, Khanwale MA (2017) Bubble generated turbulence and direct numerical simulations. Chemical Engineering Science 157:26–75
Kataoka I, Ishii M, Serizawa A (1986) Local formulation and measurements of interfacial area concentration in two-phase flow. International Journal of Multiphase Flow 12:505–529
Keane RD, Adrian RJ (1990) Optimization of particle image velocimeters. I. Double pulsed systems. Measurement Science and Technology 1:1202–1205
Langevin P (1908) Sur la théorie du mouvement brownien. Comptes-rendus de l'Académie des sciences Paris 146:530–533
Neal LG, Bankoff SG (1963) A High Resolution Resistivity Probe for Determination of Local Void Properties in Gas-Liquid Flow. AIChE Journal 9(4):490–494
Pope SB (2000) Turbulent Flows. Cambridge University Press
Revankar ST, Ishii M (1993) Theory and measurement of local interfacial area using a four sensor probe in two-phase flow. International Journal of Heat and Mass Transfer 36:2997–3007
Toombes L (2002) Experimental Study of Air-Water Flow Properties on Low-Gradient Stepped Cascades. PhD thesis, University of Queensland
Wahl TL (2003) Discussion of "Despiking Acoustic Doppler Velocimeter Data" by Derek G. Goring and Vladimir I. Nikora. Journal of Hydraulic Engineering 129:484–487
Zhang G (2017) Free-Surface Aeration, Turbulence, and Energy Dissipation on Stepped Chutes with Triangular Steps, Chamfered Steps, and Partially Blocked Step Cavities. PhD thesis, University of Queensland, DOI 10.14264/uql.2017.906